A Framework for the Visualization of Finite-Time Continuum Mechanics Effects in Time-Varying Flow

No Author Given

No Institute Given

Abstract. Integration-based flow visualization provides important visual cues about fluid transport. Analyzing the behavior of infinitesimal volumes as opposed to the behavior of rigid particles provides additional details valuable to flow visualization research. Our work concentrates on examining the local velocity gradient tensor along the path of a particle seeded within time-varying flow to produce a visualization highlighting temporal characteristics of particle behaviors, such as deformation. We present a framework for the analysis and visualization of such characteristics, focused on providing concise representations of physically meaningful flow features such as separation regions and vorticity. We apply the derived techniques to two data sets, highlighting the importance of such higher order Lagrangian analysis techniques to time-varying flow analysis.

1 Introduction

Modern flow simulations often output time-varying vector fields from which a wealth of information can be ascertained. Key techniques in visual flow analysis place particles in the flow field and follow their path as they are advected over time, thus visualizing the translational behavior of such particles.

Our work focuses on the intrinsic volumetric effects of a region of space surrounding a particle as it is advected through the field. More specifically, we are interested in secondary effects of Continuum Mechanics such as the stretching, shearing, and rotation characteristics of the flow experienced within the region. We develop a framework to isolate and visualize these individual fluid metrics, providing further insight into particle interactions within a local neighborhood. We demonstrate how a visualization of these characteristics is a crucial tool to discover and understand behaviors such as mixing.

Local instantaneous transformations of flow particles are represented by the velocity gradient tensor. To examine the transformation of a volumetric particle over a (finite) amount of time, this information has to be accumulated as it is advected through the flow field. We present a unified framework for the accumulation and visualization of a number of Continuum Mechanics effects, such as shear, stretching, and rotation. After a finite time interval, our results display the varying flow field effects that have acted on the particle. In summary, the contributions of this work to the area of flow visualization are as follows: 1) We provide a theoretical framework for a number of advanced continuum mechanics descriptors. 2) We show how existing methods fit into this framework and develop novel decriptors of particle transformations. 3) We encode and combine descriptors as scalars for visualizations that enhance the deformation traits of particles.

2 Related Work

Considerable effort has been put into identifying topological flow features into one graphical representation [1–3], commonly referred to as glyphs, by visualizing geometric primitives [4]. While our work also identifies local flow behavior, we do not aim to show all of the metrics at once. A different visualization of flow characteristics is given by work that studies higher order effects of flow fields in the form of mixing [5] and volume deformations [6, 7] induced by the velocity gradient tensor. Our work in part makes use of the flow deformation definitions given in these papers.

The use of the *Finite-Time Lyapunov Exponent* (FTLE), a measure of exponential stretching, was introduced by Haller [8] to extract salient flow features. Soon after, techniques [9][10][11] provided robust FTLE calculations along with visualizations focusing solely on flow divergence. For these works, the FTLE is calculated strictly using a flow map approach, while our work is interested in the characteristics of flow deformations experienced along the particles pathline [12]. Kasten et al. [13] introduced the notion of localized FTLE, exchanging the standard flow map gradient tensor with an accumulation of the velocity gradient tensor along pathlines.

Work has also been performed to identify the particular rotation and strain experienced during deformation. The rotation given by the velocity gradient tensor has been associated with vortex core extraction [14], while the strain component can identify shearing [15]. Both tensor components have been combined to identify flow features [16], with local strain used with FTLE for flow structure identification [17]. The visualization of local neighborhood deformation along a particle's trajectory has been captured using polygons [18], streamtubes [19], and predicates used to categorize trajectories [20][21] according to chosen flow properties. While our work also concentrates on extracting local flow field changes, the visualization accumulates these deformations into one overall image, providing a framework for identifying specific causes for contortion through arbitrary vector fields. Fuchs et al. [23] accumulate vorticity, a form of rotation, as an additional measure for vortex extraction and Obermaier et al. [22] accumulate strain, a variation of shear, in mantle flow fields for automatic strain analysis for 3D geophysical data.

Our work explores all facets of the deformation, for example magnitude, strain, and rotation within one consistent algorithmic framework. By combining the deformation experienced by a particle's neighborhood into one visualization, we can ascertain the primary fluid features along the particle's path. Furthermore, the provided results show that the examination of particle transformations in turbulent flow allows for the isolation and relation of multiple flow characteristics, thereby highlighting notable features.

3 Framework Concept

The goal of our work is to present a unified framework for the transformations experienced by particle neighborhoods moving along trajectories through the flow field. Over the lifetime of such a neighborhood, the overall deformations may be complex, but can be broken down into a set of metrics with distinct physical meanings that help explain the transformation. More specifically, we give examples of how to examine the accumulation of rotation, shear, fractional anisotropy, and stretching to better understand fluid

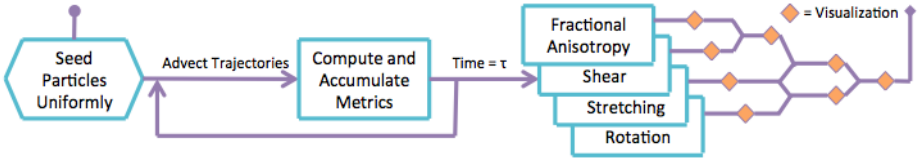

Fig. 1. Workflow of the proposed analysis and visualization framework. Particles are seeded uniformly and advected until time τ, during which the metrics are calculated and accumulated along the trajectory. These metrics can then be visualized independently or in combination.

mixing behavior. Particles are seeded uniformly throughout the data set and trajectories are advected until a time τ, during which the desired metrics are calculated and accumulated. They are then visualized at time τ both independently and in combination, as we will explore after an in-depth look at the metrics. In the next section, we describe the mathematical process involved with the calculation and accumulation of these metrics.

4 Velocity Gradient Tensors Along Trajectories

Our work explores the velocity field effects on a particle advected through the flow, specifically targeting volumetric deformations due to stretching, rotation, and shear on the particle's neighborhood (Figure 2(a)). The majority of work on post-simulation analysis focuses on fluid transport, with a much smaller subset examining in isolation, individual fluid mixing characteristics (Figure 2(b)). Our work stresses the importance of both transport and various mixing metrics, exploring how in combination, these volumetric effects give a greater insight into flow behavior. In the following, we establish the context in which we analyze the flow field and provide the required mathematical backgound. To achieve notational differentiation, vectors are denoted as bold face lower-case letters $\mathbf{v}$ to distinguish them from scalars $s \in \mathbb{R}$.

4.1 Velocity Gradient Tensor

Our main focus is on 3D velocity analysis, i.e., $\mathbf{v} = (\frac{\delta x}{\delta t}, \frac{\delta y}{\delta t}, \frac{\delta z}{\delta t})$. For our purposes, this velocity is obtained directly from a time-dependent, 3D vector field over a finite space domain $U \in \mathbb{R}^3$ and a finite temporal domain $I \in \mathbb{R}$.

To begin analysis over the entire data set, particles are seeded in a uniform distribution over all axes. Using a Runge-Kutta 4th/5th order integration scheme, the particles

Fig. 2. Volumetric Deformations. Figure (a) shows the combined effects that rotation, stretching, and shearing have on a volumetric neighborhood while Figure (b) exemplifies them individually.

are advected for a time t through the vector field v. To capture instantaneous change in a neighborhood around a particle position $\mathbf{x} = (x, y, z)$, the spatial gradient of the flow field is obtained at every time step using central differencing.

This gradient captures local changes within the flow field. As a 3×3 second-order tensor, it is a linear mapping between vectors $\mathbf{v}$ and $\mathbf{w} \in \mathbb{R}^3$. In our case, this so called *velocity gradient tensor* $\nabla\mathbf{v}$ of a flow field $v : \mathbb{R}^3 \to \mathbb{R}^3$ describes a local linearized rate of change in velocity:

$$\nabla\mathbf{v}_{ij} = \frac{\partial v_i}{\partial x_j}$$

with components corresponding to the central differencing calculation. To quantify the spatial changes given by the velocity gradient tensor, we take a closer look at its *eigenvectors* and *eigenvalues*, which give the instantaneous maximal and minimal directions and magnitude, providing principal components of the deformation.

We aim to analyze flow fields based on the transport of particles. Examining the velocity gradient tensor, instantaneous changes in the flow direction can be extracted at any point location. By calculating $\nabla\mathbf{v}$ frequently at positions along a particle's trajectory, the deformation along a specific path through the fluid is made apparent. This instantaneous change in velocity allows for the local extraction of the desired deformation descriptors. Accumulating these changes will summarize the deformations experienced by a particle throughout its lifetime, exposing flow features. In contrast to purely stationary analysis of velocity gradient components, this approach allows for the investigation of truly time-varying behaviors in a Lagrangian setting.

4.2 Neighborhood Gradient Tensor

To map the instantaneous change in velocity back to a deformation of the particle neighborhood after a single time step, consider a mapping $\mathbf{g}(\mathbf{x}) = (g_x(\mathbf{x}), g_y(\mathbf{x}), g_z(\mathbf{x})) \in \mathbb{R}^3$ that holds the position value of arbitrary points $\mathbf{x}$ in a particle neighborhood after the particle was advected for Δt. The corresponding *deformation gradient tensor*

$$\mathbf{D_{ij}} = \frac{\partial g_i}{\partial x_j}$$

is a second-order tensor describing the local deformation of line elements in space. The direct relation between velocity fields and the displacement function allows for the computation of the deformation gradient tensor $\mathbf{D}$ using the relation

$$\mathbf{D} = e^{\nabla\mathbf{v}\cdot\Delta t} \tag{1}$$

to which a first order approximation of the matrix exponential is given by $\mathbf{I} + \nabla\mathbf{v} \cdot \Delta t$. Consider a pathline $p(t) = p(\mathbf{x}, t_0; t)$ for a particle seeded at location $\mathbf{x}$ at time t_0 and advected till time t. The time evolution of the deviation of the flow field f between t_0 and t can be discretized in intervals of size Δt. Accumulating these changes, a matrix forms which holds a mapping of the neighborhood deformation at starting point $p(t_0)$ to the end point $p(t)$. $\mathbf{D}$ then describes the state of the neighborhood as a volume, allowing for volumetric analysis to quantify desired descriptors of the deformation. In this paper, we are interested in the deformation that occurs up to time t, and therefore we accumulate the deformation gradient tensor to said time.

4.3 Accumulating the Deformation Gradient Tensor

To quantify the deformation at any given time step, the effects of previous deformation gradient tensors are accumulated up to the desired time. Given an arbitrary vector $\mathbf{v}_i$ at time t_i, the effects of the deformation on $\mathbf{v}_i$ are quantified as $\mathbf{v}_{i+1} = D_i \cdot \mathbf{v}_i$ where $\mathbf{v}_{i+1}$ is the vector $\mathbf{v}_i$ after experiencing the deformation governed by $\mathbf{D}_i$. To accumulate these transformations over the lifetime of a particle, the deformation gradient tensor must be applied to the original vector $\mathbf{v}_0$ at all time steps:

$$\mathbf{v}_n = \prod_{i=0}^{n-1} D_i \cdot \mathbf{v}_0. \tag{2}$$

The deformed vector $\mathbf{v}_n$ is therefore defined by the initial vector and an accumulation of all transformations prior to step n. For an initially spherical neighborhood (input vectors $\mathbf{v}_0$ lie on the unit sphere), the accumulated deformation tensor is a direct representation of the deformed neighborhood at step n.

While this form of accumulation adds up (geometric) deformation information, other descriptors, such as scalar valued rotation must be accumulated in a slightly different form. Since an accumulated deformation will not allow for the extraction of descriptors like total rotation of a particle (due to positive and negative rotations or total rotations exceeding 2π), we extract such descriptors locally and use standard statistical measures for accumulation. Total rotation, for example, can be computed by summing up either absolute or signed local rotation angles. Similarly, average and maximal values of descriptors may be extracted along trajectories by examining local properties.

5 Scalar Descriptors of Volume Behavior

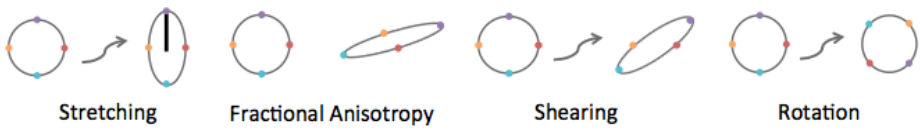

Fig. 3. Transformation effects on a spherical volume. This Figure shows the effects of stretching, shearing, and rotation on a spherical volume and also visually displays fractional anisotropy, where the left figure has a fractional anisotropy near 0 and the right near 1.

For a breakdown of the analysis process involved with a volume deformation, we first take a look at the instantaneous neighborhood itself, eliminating any temporal components. The neighborhood of a flow particle is represented abstractly in the form of a sphere, manipulated into an ellipse after experiencing a change in velocity. Let $\mathbf{E}$ be the matrix that deforms the sphere into the ellipse. The axes of the ellipse are found by extracting the singular values of $\mathbf{E}$, revealing the directions of the deformation.

By associating a velocity with the neighborhood (tangential to the particle's trajectory), we can examine in detail the forces acting on the ellipse and further distinguish

orientations. The exact combination of rotation and strain associated with the deformation is found by decomposing the velocity gradient tensor. Furthermore, by combining a sequence of these deformations, the overall change in the neighborhood can be analyzed with respect to direction and magnitude over a finite time, shown in Figure 2(b). By accumulating the deformation gradient tensor over the life-time of a particle and applying statistical measures, the total separation and rotation experienced by the local neighborhood can be quantified.

5.1 Stretching

We first begin by focusing on the magnitude of the maximal volume stretching. This notion is equivalent to how FTLE characterizes laminar and turbulent flow by measuring the separation and convergence rate of infinitesimally close particle trajectories. Given a finite-time interval, FTLE gives a measure of exponential stretching magnitude for areas of flow experiencing divergence (forward time integration) or convergence (backward time integration).

The most essential component to calculating the FTLE is the flow map gradient. In their work [13], Kasten et al. present a flow map free method for calculating the local particle deformation, replacing the flow map gradient with an accumulation of local separation measures. Without relying on a flow map, Kasten et al. presented the idea of a localized Finite-Time Lyapunov Exponent (L-FTLE) which relies solely on the local separation along an individual pathline.

Hence, over the life-time of a particle, the accumulated deformation gradient tensor can be directly applied to the calculation of the FTLE. If the tensor T_n represents the deformation accumulation after n time steps, applying the spectral norm $||\cdot||_\lambda$ to t_n gives the maximum stretching of the local neighborhood. This is equivalent to performing a singular value decomposition. Therefore, the normalized localized FTLE is defined by

$$L-FTLE(\mathbf{x},t) = \frac{1}{t}\ln(||\ T_n\ ||_\lambda) \tag{3}$$

giving a magnitude measure for the volume deformation along the pathline. Thus, the magnitude of maximal stretching is immediately encoded in the accumulated deformation gradient tensor.

5.2 Fractional Anisotropy

We are not only interested in the magnitude of stretching, but also the contortion itself. This section outlines *fractional anisotropy* (FA), which approximates how line-like a neighborhood becomes after a distortion. The FA is a scalar value between zero and one that describes the degree of anisotropy during the deformation process. A value of zero means that the deformation is fully isotropic or that it is unrestricted in all directions, see the left hand side of Figure 3 on fractional anisotropy. A value of zero may also occur if the deformation is equal in all directions. A value near one means that the deformation occurs along one axis only, see the right image of Figure 3. The equation for calculating the fractional anisotropy is

$$FA(\mathbf{T}) = \sqrt{\frac{3}{2}} \frac{\sqrt{(\lambda_1 - tr(\mathbf{T}))^2 + (\lambda_2 - tr(\mathbf{T}))^2 + (\lambda_3 - tr(\mathbf{T}))^2}}{\sqrt{\lambda_1^2 + \lambda_2^2 + \lambda_3^2}} \tag{4}$$

where $tr(\mathbf{T})$ is the normalized trace of the accumulated deformation gradient tensor and the λ's are the eigenvalues of the same tensor.

With the deformation pictured as an ellipse, the fractional anisotropy gives an idea as to how line-like the neighborhood is. A fractional anisotropy of zero would be a perfect sphere, while an FA of one would cause the ellipse to degenerate into a line. Thus, the scaling allows for two distinct filtering techniques, using the FA value to either visualize a range of deformations or to weight the importance of other flow features.

5.3 Strain and Shear

To further examine the velocity gradient tensor, we do a standard decomposition of ∇v into its symmetric component which describes the strain

$$\mathbf{S} = \frac{1}{2}(\nabla v + \nabla v^T) \tag{5}$$

where $S_{ij} = \frac{1}{2}\left(\frac{\delta u_i}{\delta x_j} + \frac{\delta u_j}{\delta x_i}\right)$ and rotational components equate to zero. When considering strain in fluid mixing, we are most interested in the shearing force driving the deformation. Shear occurs when two or more infinitesimally close vectors within the flow field f are parallel but of different magnitude. Particles seeded on these vectors travel along trajectories parallel to one another while the distance between them increases, see Figure 3. To give a measure for the difference in the vector field magnitude causing the shearing, the angle between the direction of strain and the direction of the particle is found [15]. It is important to distinguish shearing from other types of divergence in order to properly identify flow separation. Eliminating the rotational component of deformation, the maximum eigenvector of Eq. (5) will give the desired strain direction.

While the angle between the strain and particle direction provides a metric for shearing magnitude in 2D, it may not capture all shearing cases that occur in 3D. If the majority of the strain force is equally distributed along two of the three axes, while a smaller strain is experienced in the third, the maximum eigenvector of the strain tensor would give an arbitrary direction. To isolate the strain magnitude in 3D, we take a different approach, looking at the force of separation. Because we are most interested in deformation effects along a pathline, the greatest effect from a separation force would occur on the plane orthogonal to the particle direction. This plane can be found using the particle's position and its velocity as the plane normal. The separation magnitude along this plane is then just the largest eigenvalue of the projected deformation tensor. Shear is represented as $SEP(\mathbf{T}_S)$ at each time step where $\mathbf{T}_S$ is the strain component of the deformation tensor. The accumulation of this metric is done by taking the average of the shear over all time steps.

5.4 Rotation

Completely eliminating separation forces, the anti-symmetric part of the velocity gradient tensor focuses on rotation. Decomposing ∇v into its anti-symmetric component

describes the deformation due to rotation:

$$\Omega = \frac{1}{2}(\nabla v - \nabla v^T) \tag{6}$$

where $\Omega_{ij} = \frac{1}{2}\left(\frac{\delta u_i}{\delta x_j} - \frac{\delta u_j}{\delta x_i}\right)$ which is commonly referred to as the *vorticity* or the tendency of particles in a fluid to rotate (Figure 3). The length of this vector gives the angular velocity of the rotation.

In a 2D setting, the vorticity describes the rotation on the plane itself and the accumulation of this metric gives total rotation of a particle around the z-axis. However, in 3D the physical meaning becomes unclear with respect to the pathline as the axis of rotation may change at every time step. Accumulating the angular velocity would have no clear meaning seeing as every plane of rotation could vary. Instead, we have chosen to focus on the twisting a particle experiences while traveling along its trajectory. In other words, we are interested in the angular velocity on the plane orthogonal to the pathline. Therefore, the deformation gradient tensor is projected onto this plane and the projection is then substituted into Eq. (6) for the calculation of vorticity. Summing the absolute vorticity at every time step now serves to show how the particle twirls along its trajectory, referred to as $ROT_A(\mathbf{T}_\Omega)$ where $\mathbf{T}_\Omega$ is the anti-symmetric component of the accumulated deformation tensor [19].

6 Metric Combination

Even when given only the basic characteristics of flow deformation, their combination can further the analysis of the fluid flow. Beginning with the strain component of the velocity gradient, the separation can be broken down into three cases. In the first case, shearing occurs along the particle's flow direction, thereby resulting in a low separation magnitude on the plane orthogonal to the particle's velocity vector. A high separation magnitude results from shearing that occurs orthogonal to the flow direction, categorized here as the second case. The final case occurs when there is no notable shearing, resulting in a median separation magnitude, irrelevant to the metric purpose. However, this third case can be isolated using the fractional anisotropy. Volumetric tensor effects having a fractional anisotropy near 0 also categorize those volumes that experience little to no shearing. Weighting the shearing metric by fractional anisotropy using the following equation:

$$SEP_{FA}(\mathbf{T}_S) = FA(\mathbf{T})^3 \times SEP(\mathbf{T}_S) \tag{7}$$

filters out the third case from the separation metric. Furthermore, this filtered separation can then be applied to the divergence rate found by FTLE.

Recall that the FTLE gives the maximum separation rate of infinitesimally close particle trajectories over a finite time, referred to here as the maximum separation magnitude of the neighborhood surrounding a particle along its trajectory. While certain methods, especially Lagrangian Coherent Structure extraction, focus on the separation due to changes in flow direction, FTLE is also sensitive to changes in flow magnitude (Please refer to [15] for an in-depth explanation). The change in flow magnitude is isolated by the separation magnitude due to shearing. Therefore, filtering the FTLE by the

SEP_{FA} metric can better express FTLE in terms of changes in flow direction. This is done by a direct linear filtering after the accumulated shearing magnitudes are normalized between 0 and 1:

$$FTLE_A(\mathbf{T}) = SEP_{FA}(\mathbf{T}_S) \times FTLE_A(\mathbf{T}) \tag{8}$$

where $FTLE_A(\mathbf{T})$ is the separation rate of the accumulated tensor $\mathbf{T}$ along the trajectory.

Applying the rotation metric to FTLE can also provide insight into the flow field. Directly combining both metrics:

$$PLANAR\_SEP(\mathbf{T}) = FTLE_A(\mathbf{T}) + ROT_A(\mathbf{T}_\Omega) \tag{9}$$

reveals the maximum separation due to planar separation.

7 Results

In the following we present examples that illustrate the velocity gradient-based descriptors extracted with our technique. We study these metrics using two time-varying data sets, one depicting a jet flow and the other a Karman vortex street. The Jet Flow data set has dimensions $128 \times 256 \times 128$, while the Karman data set is of size $167 \times 34 \times 34$. Both are represented as uniform grids. Particles are seeded uniformly to cover all grid spaces and are advected using Runge-Kutta 4th/5th order integration for a time $T = 5$. The velocity gradient tensor is calculated 10 times per time step (a total of 50 per trajectory), using central differencing. The deformation gradient tensor is then accumulated, along with shear and rotation statistical measures. With respect to performance, the additional workload of computing the velocity gradient and solving for the eigenvectors and eigenvalues is nominal compared to the traditional computational load associated with finding nearest neighbors for pathline advection, i.e. cell location. All images were created using the Voreen volume visualizer [24].

7.1 Shear and Fractional Anisotropy

To visualize shearing effects, we compute the separation magnitude due to shearing in the flow, choosing to compute this magnitude on the plane orthogonal to the particle's trajectory. Mentioned earlier, this descriptor also provides magnitudes in areas of little to no shear, giving the magnitude of the overall volumetric effect of the tensor, shown in Figure 4(d). These particular values are given a slight cyan opacity to show that these values occur in areas outside of the flow structure boundary. Filtering the shearing magnitude by the fractional anisotropy (SEP_{FA}) eliminates the unwanted shear magnitudes, giving way to Figure 4(b). Stretching orthogonal to the flow direction is shown in purple, while stretching along the particle's trajectory is shown in orange. From the image we see that the highest amount of shearing along the particle's trajectory occurs in the middle of the plume, relaying the difference in magnitude as the flow billows from the jet. The highest amount of shearing orthogonal to the trajectory is shown to occur on the outside of the plume, outlining areas where the moving flow from the jet interacts with the still surroundings, causing vortex-like features. Fractional anisotropy can also

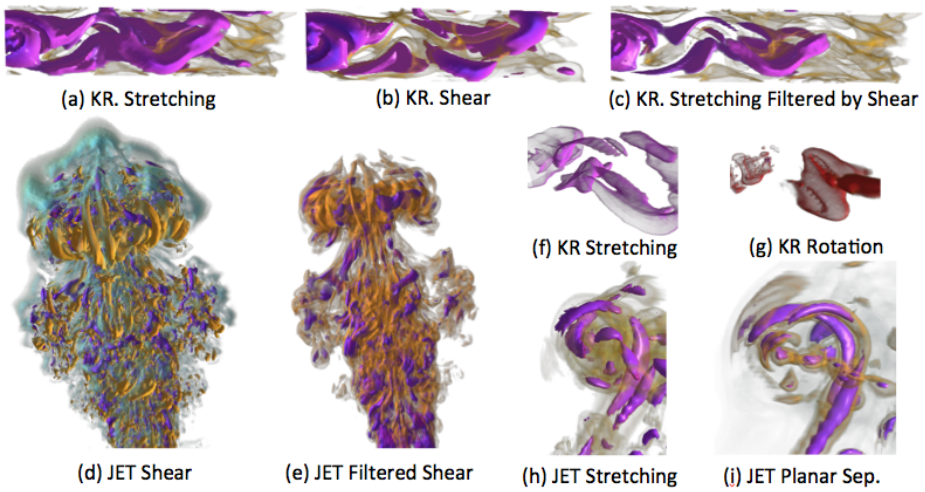

Fig. 4. Karman (KR) and Jet data sets (Low - cyan, mid - orange, high - purple). (a) shows mid to high FTLE values. (b) shows the shearing descriptor, already filtered by fractional anisotropy. (c) shows the filtering of FTLE to eliminate divergence due to shearing, clearly displaying the two manifolds. (d) shows the separation magnitude due to shearing. Shearing along the particle's trajectory is shown in orange, orthogonal shearing in purple, and areas of no shearing shown in cyan. (e) shows the same shearing descriptor filtered by fractional anisotropy to eliminate areas of no shear. (f) shows the FTLE which clearly discerns between two manifolds formed by flow going over and under the obstacle. (g) shows the rotation (in red) that occurs when particles following the divergence of both manifolds meet and rotate due to differences in speed. (h) shows the FTLE metric of the top of the plume hinting at rotation. (i) exposes the rotating flow features in more detail by showing planar separation.

be used as a filter for FTLE in compressible data sets, allowing to distinguish between divergence and uniform expansion.

While providing insightful information into the fluid flow on its own, the shearing magnitude can also be used as a filter for the stretching magnitude found using the FTLE. In certain applications, flow divergence due to time-varying separation is preferred over general flow divergence. However, the FTLE does not distinguish between the two. Filtering the FTLE by the separation magnitude due to shearing can eliminate the later component due only to differences in flow magnitude ($FTLE_A$). Figure 4(a) shows the FTLE metric of the Karman data set, with mid to high values generously covered in purple. Figure 4(b) shows the separation magnitude due to shearing, already filtered by fractional anisotropy. Following the filtering scheme described in Section 6, the result of filtering the FTLE descriptor by the shear descriptor is shown in Figure 4(c). The exact same volume transfer function is used in both 4(a) and 4(c), highlighting the same range of FTLE values in purple, instantly revealing the two distinct manifolds in the latter by eliminating divergence due to shearing. This filtering technique can be applied to the mixing of multiple fluids, capturing the boundary between them caused by a difference in velocity during fluid interaction, while eliminating the separation due to shear slightly beyond the boundary layer.

7.2 Rotation and Stretching

Rotation is not synonymous with stretching and therefore can illustrate flow effects not present in an FTLE-based visualization, a method favored for the visual classification of turbulent flow. Particles that diverge according to the two prominent manifolds in the Karman data set should, in theory, meet and interact. If one front moves faster than the other, this interaction should result in a rotation. Figure 4(f) shows only the flow divergence in purple, while Figure 4(g) shows only rotation in red. This image shows rotation occurring when the particles following the two divergence structures interact, confirming the theory. Being able to identify such isolated rotating pockets is crucial for the analysis and optimization of mixing processes, where such islands tend to degrade mixing quality.

The jet flow data set, more turbulent than the Karman, does not often have areas where rotation is completely separate from stretching. Therefore, the planar separation (*PLANAR_SEP*) is a more interesting measure, combining the stretching and rotation descriptors. Figure 4(h)(i) shows two images side by side, both of the same area covering a section of the plume. Figure 4(h) is the FTLE while Figure 4(i) shows high values of planar separation. All high values are colored purple for both. By extracting the planar separation, the rotational separation formed by the plume when it closes in on itself is better displayed, connecting the divergence structures in question. Figure 4(i) visualizes the twisting effects experienced by particles traversing the plume.

8 Conclusion and Future Work

We have presented a unified framework for the identification and extraction of meaningful flow features along a particle's trajectory as it passes through a time-varying vector field. Adding to the commonly studied transport of fluid, we have shown that measuring rotation and shear along a particle's trajectory can give insight into the mixing behavior. Furthermore, coupled with flow divergence, these metrics help identify specific areas of interest, highlighting areas of divergence due to shearing and observing areas of lower divergence with an emphasis on rotation.

We plan to extend this work to methods that use the velocity gradient as a building block in a Lagrangian setting. The metrics we have chosen to focus on are not the only meaningful characteristics of flow deformation that can be extracted from the velocity gradient tensor. For instance, Lagrangian Coherent Structures (LCS) and vortex cores are detected using components of the velocity gradient tensor. Along with an extension to other gradient methods, we plan to explore various flow visualization techniques for the deformation metrics to better combine them with the method's results.

References

1. Globus, A., Levit, C., Lasinski, T.: A tool for visualizing the topology of three-dimensional vector fields. In: IEEE Conf. on Vis., 1991. (1991) 33 –40, 408
2. Ropinski, T., Oeltze, S., Preim, B.: Visual computing in biology and medicine: Survey of glyph-based visualization techniques for spatial multivariate medical data. Comp. and Graph. **35** (2011) 392–401

3. Wiebel, A., Koch, S., Scheuermann, G.: Glyphs for non-linear vector field singularities. In: TopoInVis. Springer Berlin Heidelberg (2012) 177–190
4. de Leeuw, W.C., van Wijk, J.J.: A probe for local flow field visualization. In: Proc. of the 4th Conf. on Vis. '93. (1993) 39–45
5. Haller, G.: Finding finite-time invariant manifolds in two-dimensional velocity fields. CHAOS **10** (2000) 99–108
6. Obermaier, H., Hering-Bertram, M., Kuhnert, J., Hagen, H.: Volume deformations in gridless flow simulations. Comp. Graph. Forum **28** (2009) 879–886
7. Obermaier, H., Joy, K.I.: Derived metric tensors for flow surface visualization. IEEE Trans. on Vis. and Comp. Graph. **18** (2012) 2149–2158
8. Haller, G.: Distinguished material surfaces and coherent structures in three-dimensional fluid flows. Physica D: Nonlinear Phenomena **149** (2001) 248 – 277
9. Sadlo, F., Peikert, R.: Visualizing lagrangian coherent structures and comparison to vector field topology. In: TopoInVis. (2007)
10. Garth, C., Gerhardt, F., Tricoche, X., Hagen, H.: Efficient computation and visualization of coherent structures in fluid flow applications. IEEE Trans. on Vis. and Comp. Graph. **13** (2007) 1464 –1471
11. Garth, C., Wiebel, A., Tricoche, X., Joy, K., Scheuermann, G.: Lagrangian visualization of flow-embedded surface structures. Comp. Graph. Forum **27** (2008) 1007–1014
12. Theisel, H., Weinkauf, T., Hege, H.C., Seidel, H.P.: Topological methods for 2d time-dependent vector fields based on stream lines and path lines. IEEE Trans. on Vis. and Comp. Graph. **11** (2005) 383–394
13. Kasten, J., Petz, C., Hotz, I., Noack, B.R., Hege, H.C.: Localized finite-time lyapunov exponent for unsteady flow analysis. In: VMV. (2009) 265–276
14. Jiang, M., Machiraju, R., Thompson, D.: Detection and visualization of vortices. In: The Vis. Handbook, Academic Press (2005) 295–309
15. Pobitzer, A., Peikert, R., Fuchs, R., Theisel, H., Hauser, H.: Filtering of FTLE for visualizing spatial separation in unsteady 3d flow. In Peikert, R., Hauser, H., Carr, H., Fuchs, R., eds.: TopoInVis, Springer (2012) 237–253
16. Haimes, R., Kenwright, D.: On the velocity gradient tensor and fluid feature extraction. Technical Report AIAA Paper (1999)
17. Kasten, J., Hotz, I., Hege, H.C.: On the elusive concept of lagrangian coherent structures. In: TopoInVis. Springer Berlin Heidelberg (2012) 207–220
18. Schroeder, W.J., Volpe, C.R., Lorensen, W.E.: The stream polygon: a technique for 3d vector field visualization. In: Proc. of the 2nd conf. on Vis. '91, IEEE Computer Society Press (1991) 126–132
19. Ueng, S.K., Sikorski, C., Ma, K.L.: Efficient streamline, streamribbon, and streamtube constructions on unstructured grids. IEEE Trans. on Vis. and Comp. Graph. **2** (1996) 100 –110
20. Salzbrunn, T., Scheuermann, G.: Streamline predicates. IEEE Trans. on Vis. and Comp. Graph. **12** (2006) 1601 –1612
21. Salzbrunn, T., Garth, C., Scheuermann, G., Meyer, J.: Pathline predicates and unsteady flow structures. The Visual Comp. **24** (2008) 1039–1051
22. Obermaier, H., Billen, M.I., Hagen, H., Hering-Bertram, M., Hamann, B.: Visualizing strain anisotropy in mantle flow fields. Comp. Graph. Forum (2011) 2301–2313
23. Fuchs, R., Peikert, R., Sadlo, F., Alsallakh, B., Gröller, E.: Delocalized unsteady vortex region detectors. In: VMV. (2008) 81–90
24. Meyer-Spradow, J., Ropinski, T., Mensmann, J., Hinrichs, K.H.: Voreen: A rapid-prototyping environment for ray-casting-based volume visualizations. IEEE Comp. Graph. and App. **29** (2009) 6–13